Journal of Materials Chemistry A

RSC Publishing

COMMUNICATION

View Article Online
View Journal | View Issue

Cite this: *J. Mater. Chem. A*, 2013, **1**, 203

Received 4th October 2012
Accepted 19th October 2012

DOI: 10.1039/c2ta00558a

www.rsc.org/MaterialsA

Graphitic domain layered titania nanotube arrays for separation and shuttling of solar-driven electrons†

Dong Ki Lee,[a] Kyu Sung Han,[a] Weon Ho Shin,[a] Jung Woo Lee,[a] Jung Hoon Choi,[a] Kyung Min Choi,[a] Yeob Lee,[a] Hyoung-il Kim,[d] Wonyong Choi[d] and Jeung Ku Kang*[abc]

Herein, we report a facile method for synthesizing graphitic carbon domains of thin island shapes on the surfaces of titania nanotubes, which were prepared by using hydrothermal and pyrolytic treatments with glucose. The faster decay time of the solar-driven electrons and the lower charge transport resistance on carbon domains as compared to those in the case of bare titania nanotubes serve to increase the solar-to-hydrogen conversion rate.

After excitation of an electron from the valence band (VB) to the conduction band (CB) of a semiconductor, the electron separated from the electron–hole pair has a short lifetime because of its strong tendency to recombine with the hole. Thus, only a few electrons from the semiconducting photocatalyst can participate in the reduction reaction. This is the critical bottleneck in the conversion of solar energy to a high-density energy carrier such as hydrogen.[1–8] Meanwhile, structures combined with graphitic carbon allotropes have been found to be useful in facilitating the separation of solar-driven electrons.[9–11] Photoexcited electrons in TiO_2 were found to move into the attached graphitic carbon because the Fermi level of that is lower than the CB of TiO_2, and delocalized π-orbitals are allowed to store electrons and provide easy transport.[12–14] These effects resulted in the efficient suppression of charge recombination in TiO_2.[15] However, combining graphitic carbon allotropes with multidimensional structured semiconductors such as ordered nanotube (NT) arrays is still a great challenge because of their restrictive growth conditions. In principle, electrons can be efficiently separated from electron–hole pairs and then shuttled to hydrogen protons through the creation of sp^2-bonded carbon layers with nanometer-scale sizes on the surfaces of semiconductors (Scheme 1d). Herein, we demonstrate a facile method for synthesizing thin island-shaped graphitic domains (GDs) from a network of graphitic carbon layers on the surface of TiO_2 NTs, prepared by using hydrothermal and pyrolytic treatments with glucose. Two to four surface-aligned sp^2-bonded carbon layers give the solar-driven electrons of TiO_2 a long decay time (separation) and low charge transport resistance (shuttling), which result in an increase in the solar-to-hydrogen conversion rate.

Hydrothermally polymerized glucose was employed as the source of the GDs because of its several advantages: (i) it is easy to form the polymerized glucose layers using this process without any structural constraint, and (ii) rearrangement of the C atoms from tangled chains to an ordered structure is possible through the removal of non-carbon elements by pyrolysis.[16,17] The growth of the

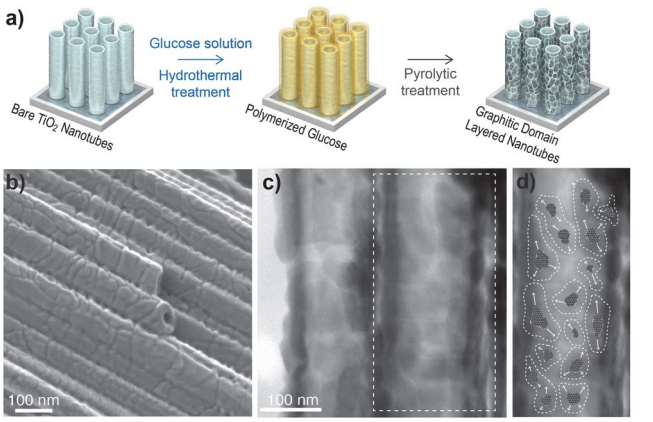

Scheme 1 (a) Schematic representation of processes for synthesizing graphitic domains (GDs) on TiO_2 nanotube (NT) arrays. (b) FE-SEM image and (c) STEM image for the side view of the GD layered TiO_2 NTs. (Top view is in Fig. S1d.†) (d) Schematic description of the pyrolytic growth process for the GDs in the white box in (c).

[a]*Department of Materials Science & Engineering, Korea Advanced Institute of Science and Technology (KAIST), 291 Daehak-ro, Yuseong-gu, Daejon 305-701, Republic of Korea. E-mail: jeungku@kaist.ac.kr; Fax: +82-42-350-3310; Tel: +82-42-350-3378*

[b]*Graduate School of EEWS (WCU), Korea Advanced Institute of Science and Technology (KAIST), 291 Daehak-ro, Yuseong-gu, Daejon 305-701, Republic of Korea*

[c]*NanoCentury KAIST Institute, Korea Advanced Institute of Science and Technology (KAIST), 291 Daehak-ro, Yuseong-gu, Daejon 305-701, Republic of Korea*

[d]*School of Environmental Science and Engineering, Pohang University of Science and Technology (POSTECH), Pohang, 790-784, Korea*

† Electronic supplementary information (ESI) available: Experimental and additional information regarding SEM, TEM, XPS, Raman, UV-vis absorbance spectra, TCSPC, EIS, and hydrogen evolution of GDNs. See DOI: 10.1039/c2ta00558a

GDs started with the pyrolytic decomposition of glucose, and they are found to grow preferentially at convex sites on the TiO_2 NTs instead of concave sites; bare TiO_2 NTs have uneven surfaces (Fig. S1b†) because of the annealing process used to transform them to the anatase phase.[18–21] Therefore, rearrangement of the C atoms proceeds as the GDs spread out along the TiO_2 NTs from the convex points (Scheme 1d). In consequence, this mechanism leads to isolated shapes with nanometer-scale sizes on concave sites with distinct intervals between them (Scheme 1b), whereas polymerized glucose forms a continuous cover (Fig. S1c†).

Formation of island-like GDs along the curved surface of a TiO_2 NT was confirmed in the GDN-5 (Graphitic Domain Layered Nanotube-5, glucose 50 mmol and pyrolyzed at 650 °C; see the experimental conditions for the various samples in Table S1 in the ESI†) sample by field-emission scanning electron microscopy (FE-SEM, Scheme 1b) and scanning transmission electron microscopy (STEM, Scheme 1c). The FE-SEM image shows that GDs are separated through cracks on the surface of the TiO_2 NT, and the contrast between the light and dark regions in the STEM image indicates that the average size of GDs is about 20–30 nm.

The high-resolution transmission electron microscopy (HR-TEM) image in Fig. 1b shows that the GD consists of two to four interface-aligned carbon layers on the surface of the anatase NT. Their irregular *d*-spacings of 0.333, 0.341, and 0.371 nm match with those for graphite (0.335 nm) or stacked multilayer graphene (0.377 nm). This demonstrates that the carbon layers are partially made up of continuous sp^2-hybridized C atoms, although irregular (Fig. S2a†), thick and fragmented (Fig. S2b†) carbon layers are observed at some points on the NT in Fig. 1a. The FE-SEM image in Fig. S1d† shows that the original morphology of the TiO_2 NT was maintained after formation of the GDs, while its interface was slightly modified upon binding to the GDs, as seen in the X-ray diffraction (XRD) patterns (Fig. 2c).

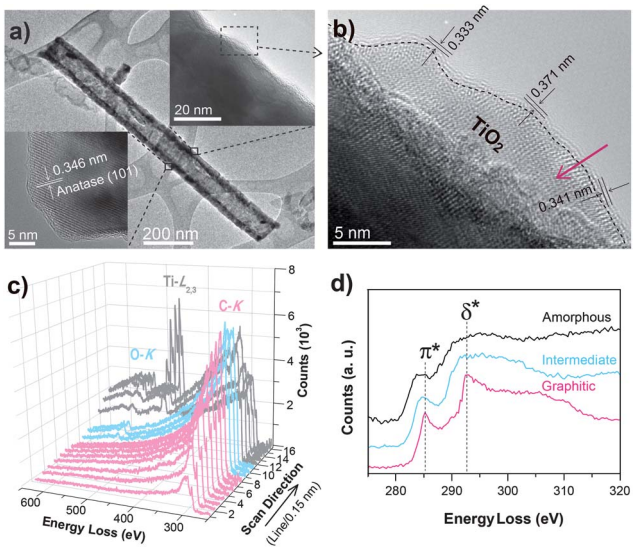

Fig. 1 (a) HR-TEM image of a single tube in GDN-5. The bottom inset shows the anatase phase. (b) High-magnification image of the black square in the top inset in (a). The two to four sp^2-hybridized C layers cover the TiO_2 NT. (c) EELS spectra. The scanning site and the direction are shown with the red arrow in (b). (d) C K-edge spectra for different states of carbon layers. The red line is line 8 in the EELS spectra in (c). Black and blue lines correspond to the black arrows in Fig. S2c and d,† and blue arrows in Fig. S2a and b,† respectively.

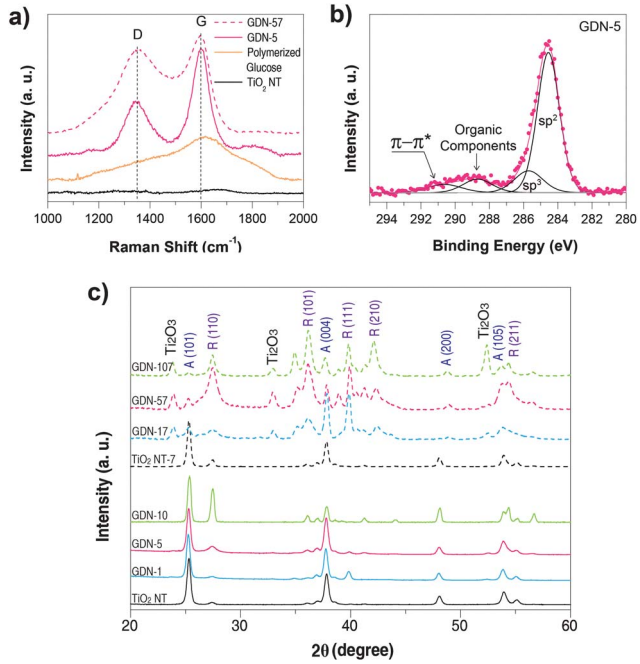

Fig. 2 (a) Raman spectra in the 1000–2000 cm^{-1} range. The I_D/I_G values of GDN-5 and GDN-57 are 0.56 and 0.86, respectively. (Raman spectra of GDN-1 and GDN-10 are shown in Fig. S4.†) (b) XPS C 1s spectrum of GDN-5. (XPS spectra of other samples are shown in Fig. S3.†) (c) XRD spectra of all samples (A for anatase, R for rutile and Ti_2O_3 for various titanium oxides). GDN-5 had a preserved anatase phase similar to that of bare TiO_2 NT. The phase transition from the anatase to the rutile is accelerated by increase in the glucose concentration and pyrolysis temperature.

Electron energy loss spectroscopy (EELS) profiling in Fig. 1c shows the electronic states of the C, O, and Ti atoms in the GD (lines 1–8, magenta), the interface junction (lines 9–11, blue), and the TiO_2 NT (lines 12–16, gray). The C K-edge signals show sharp and well-separated π* (285 eV) and σ* (292 eV) excitation peaks continuously along the scanning direction within the 0.9 nm range (lines 3–9), which is consistent with three stacked layers of C atoms. It is also observed that the overall shape of the C K-edge peaks gradually becomes round and irregular at the region of the junction with TiO_2 (around line 10), where very weak oxygen K-edge peaks are observed. The red line in Fig. 1d is a single C K-edge spectrum corresponding to line 8 in Fig. 1c. In addition, the C K-edge spectra of carbon layers in the intermediate (Fig. S2a and b†) and amorphous (Fig. S2c and d†) states were also determined, as shown by the blue and black lines in Fig. 1d, respectively. The overall peak shapes of the GDs have vivid excitation peaks and a tail over 295 eV which resembles the graphite spectrum,[22] which is clearly distinguished with relatively disordered carbon in amorphous regions. As the degree of disorder increases, the π* peak becomes blunter and shifts to the left, while the σ* peak becomes rounder and its tail becomes bigger. Meanwhile, since the TiO_2 NT is thicker and larger (140 nm diameter and 25 nm wall) than the GD, the C K-edge peaks in the TiO_2 NT region (around line 14) are not as fine as before (lines 1–11), whereas the very strong signals for the anatase phase (around line 12) show

Ti $L_{2,3}$-edge (459 and 465 eV), O K-edge (538 and 542 eV), and Ti L_1-edge (567 eV) peaks.[23]

To determine the states of the C atoms in the GDs, Raman spectroscopy and X-ray photoelectron spectroscopy (XPS) measurements were also performed. The Raman spectrum of the polymerized glucose covered TiO_2 NTs shows a very broad arc within the 1100–1900 cm^{-1} range, and a slightly convex peak is observed in the G-band (Fig. 2a). These results show that it is in a gel state with a cross-linked chain network (Fig. 1a and S1c†).[24,25] After pyrolytic treatment, GDN-5 showed two clear peaks at 1598 and 1351 cm^{-1} matching the G-band (E_{2g} mode) and the D-band (A_{1g} mode), respectively. Although the two peaks are rounder than those for common graphite or graphene, the relative ratio of the D-band intensity to the G-band intensity ($I_D/I_G = 0.56$) indicates that the C atoms in GDN-5 are sp^2 hybridized.[26–28] In general, the rise of the D-band intensity demonstrates an increase in the degree of the disorder of the carbon. In addition, it can be interpreted with following meanings: (i) GDs have unavoidable disorder because they do not exist as continuous planes, but rather as curved islands with irregular sizes because of the pyrolytic growth process (Scheme 1d), and (ii) non-sp^2-hybridized C atoms can exist at the boundaries and contact sites between the carbon layers of the GDs because C atoms have their own individual orientations along the surface curvature of the NT. Consequently, it is expected that the shifts in the peak positions of the G-band and the D-band as compared to those of graphite or graphene are caused by these disorder of the carbon. Meanwhile, the intensity of the D-band peak for GDN-57 (glucose 50 mmol and pyrolyzed at 750 °C) is remarkably higher ($I_D/I_G = 0.86$) than GDN-5, which can be attributed to the collapse of the tubular morphology of TiO_2 (Fig. S1f†) as C atoms penetrate into the anatase crystal above the 700 °C temperature for the transition from the anatase phase to the rutile phase as seen in Fig. 2c.[20] These results indicate that the polymerized glucose in GDN-57 grows only into small lumps of amorphous carbon.

The XPS results (Fig. 2b and S3†) were also consistent with the Raman measurements. The peaks of the C 1s spectra located at 284.6, 285.8, and 288.5 eV represent the sp^2- and sp^3-hybridized C atoms and the sum of the C atoms in O-containing groups (denoted as organic components) such as ether (C–O), carbonyl (C=O), and carboxyl (O–C=O) groups, respectively.[29–31] The C 1s spectrum of polymerized glucose has a shape similar to that of common glucose spectra (Fig. S3†). However, GDN-5 has a stronger sp^2 peak and weaker sp^3 and organic component peaks. In addition, only GDN-5 shows a π–π^* shake-up satellite (290.7 eV) indicating that a π electron transition occurs from occupied to unoccupied valence orbitals. These results demonstrate that most of the carbons in GDN-5 accommodate electrons in the delocalized orbitals created by hybridization of p orbitals. However, GDN-57 has strong sp^3 and organic component peaks without any π–π^* peak, indicating that a rigid structural support is needed for the growth of a graphitic carbon layer.

The preservation of anatase-phase TiO_2 NTs with good photocatalytic properties is important because the GDs themselves cannot produce solar-driven electrons. During the pyrolytic treatment, changes in the crystal structure and morphology of the TiO_2 NTs are induced by rearrangement of the C atoms of the polymerized glucose on the surface. These changes are accelerated by increase in the glucose concentration or the pyrolysis temperature. The bare TiO_2 NTs have polycrystalline anatase crystal structures with (101), (004), (200), and (105) orientations, as seen in Fig. 2c. The intensities for the (110), (101), and (111) rutile peaks are found to be slightly increased for increased glucose concentration under the 650 °C pyrolysis condition (GDN-1 and GDN-5). However, strong rutile peaks and various titanium oxides (denoted as Ti_2O_3) are observed for the 750 °C pyrolysis condition (GDN-17, GDN-57, and GDN-107), along with the disappearance of the anatase peaks. This is because C atoms of the polymerized glucose can penetrate into the TiO_2 crystal during the transformation from the anatase to the rutile phase. Meanwhile, a Ti–C bond peak (281.8 eV) is found in GDN-10 (Fig. S3†), which has a higher amount of carbon and a stronger rutile peak than GDN-1 and GDN-5. These results indicate that a high temperature and an excess of carbon force the O atoms to be replaced with C atoms in TiO_2. In addition, the diffuse ultraviolet-visible (UV-vis) absorbance spectroscopy result also shows a similar case (see Fig. S5†).

The enhancement of the photocatalytic properties due to the GDs was determined using time-correlated single-photon counting (TCSPC) and electrochemical impedance spectroscopy (EIS) measurements. In the fluorescence spectra, as shown in the inset of Fig. 3a, the bare TiO_2 NT (black), platinum (Pt)-coated TiO_2 NT (TiO_2 NT:Pt, gray) and GDN-5 (red) were found to have the same emission edge at 509 nm. The TiO_2 NT:Pt was also compared for the ability of charge separation by the GDs, where the Pt layers on the bare TiO_2 NT were prepared using the Pt sputtering at 50 W for 1 minute. We found that the TiO_2 NT:Pt shows a lower intensity of the

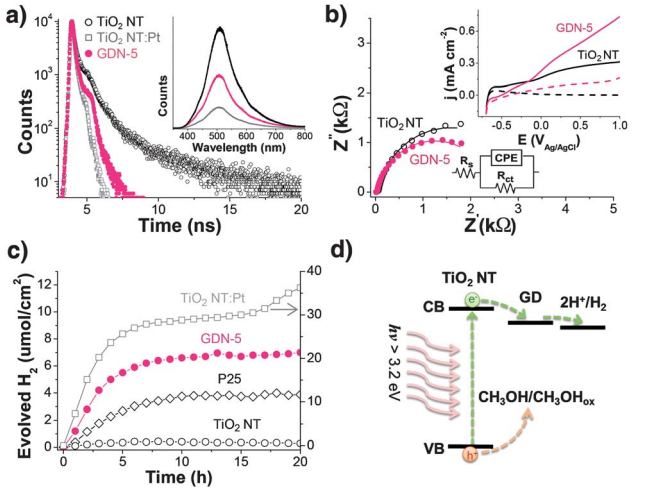

Fig. 3 (a) Fluorescence decay spectra of bare TiO_2 NTs, the Pt coated TiO_2 NT (TiO_2 NT:Pt) and GDN-5 measured by the TCSPC. The detailed fitted data are presented in Table S2.† The fluorescence spectra of each sample (TiO_2 NT: black, GDN-5: red and TiO_2 NT:Pt: gray) are shown in the inset. (b) The EIS Nyquist plot under AM 1.5G conditions at open-circuit potential. An aqueous solution of 0.1 M $NaClO_4$ with 25 vol% methanol was used as the electrolyte. The tri-exponential function fitted parameters are listed in Table S3.† The inset shows voltammograms of GDN-5 and TiO_2 NT under same conditions with EIS measurement. The dotted lines are dark currents. (d) Hydrogen evolution results from a water solution of 25 vol% methanol in the closed-circulation system (P25: 20 mg P25 was used under the same conditions). The *y*-axis at the right side is only for TiO_2 NT:Pt.

fluorescence edge and a faster decay spectrum at 509 nm (Fig. 3a) compared to those of the bare TiO_2 NT. This is considered to be the decorated Pt layer quickly absorbing photoexcited electrons from the CB of the TiO_2 before the natural fluorescence decay or recombination occurs.[32] For this reason, the average lifetime of charge carriers in the bare TiO_2 NT (3.36 ns) became more faster to 0.91 ns by the Pt (the data fitted with a tri-exponential function in Table S2†). Also, a short lifetime of 1.89 ns by GDN-5 demonstrates that the coated GDs help to quickly separate photoexcited electrons before the recombination with holes. This is because the Fermi level referenced to the normal hydrogen electrode (NHE) of the graphitic carbon layers of the GDs (−0.4 to 0.0 eV *vs.* NHE)[33,34] is lower than the CB of a bare TiO_2 nanotube (−0.5 eV *vs.* NHE).

Moreover, the EIS measurement was carried out because it provides the information on the interfacial charge transfer between the semiconducting electrode and the electrolyte.[35] Fig. 3b shows a Nyquist plot at the open-circuit potential. The Pt and Ag/AgCl electrodes were used as counter and reference electrodes, respectively. The equivalent circuit model containing the constant phase element (CPE) was employed to calculate EIS parameters, including the initial total resistance working electrode (R_s) and the TiO_2–electrolyte or TiO_2–GD–electrolyte interface charge transfer resistance (R_{ct}).[36–38] The R_s value of GDN-5 was decreased, attributed to the graphitic carbon layers of GDs having the low electrical resistance than that for TiO_2. The R_{ct} values corresponding to bare TiO_2 NTs and GDN-5 are 3023 Ω and 2419 Ω, respectively (Table S3†). This clarifies that the graphitic carbon layers in GDN-5 promote the shuttling of solar-driven electrons from the TiO_2 to the electrolyte. The inset in Fig. 3b shows the voltammogram of bare TiO_2 NTs and GDN-5, where it has been scanned from −0.7 V to 1 V. It shows that the GDN-5 results in a large amount of current density compared to that of a bare TiO_2 NT by incident photons. However, GDN-5 has a low current density at a voltage below about −0.19 V than that for a bare TiO_2 NT. This occurs since photoexcited electrons from TiO_2 could not transport stably into the Pt counter electrode as the GDs on the surface of a TiO_2 NT play as efficient electron transfer centers.[39]

Moreover, the solar-to-hydrogen conversion rates were also evaluated by measuring the hydrogen evolution from a water solution of 25 vol% methanol in a closed-circulation system with the gas chromatograph (GC). The graphitic carbon layers of the GDN-5 have a lower Fermi level than the CB of TiO_2; thus the separated solar-driven electrons in the GDs can reduce hydrogen protons in water at the interface, as schematically described in Fig. 3d. Meanwhile, the remaining holes in TiO_2 could be consumed by a scavenger such as methanol[40–42] primarily at the exposed TiO_2 surface neighboring to the GDs. Indeed, Fig. 3c shows that GDN-5 results in a high conversion rate of solar energy into hydrogen of 6.7 μmol cm^{-2} h^{-1} than 0.41 μmol cm^{-2} h^{-1} for a bare TiO_2 NT. Meanwhile, the hydrogen conversion rates of TiO_2 NT:Pt and P25 (20 mg) were 29.4 μmol cm^{-2} h^{-1} and 3.8 μmol cm^{-2} h^{-1}, respectively. The conversion rate of GDN-1 (0.54 μmol cm^{-2} h^{-1}) is similar to that of a bare TiO_2 NT as the amount of polymerized glucose is very low to create a graphitic carbon layer. Indeed, XPS (Fig. S3†) and Raman (Fig. S4†) analyses demonstrate that the state of the carbon in GDN-1 is quite similar to that of the carbon contaminating bare TiO_2 NTs. Also, GDN-10 (1.9 μmol cm^{-2} h^{-1}) with thick (Fig. S1e†) and amorphous (Fig. S4†) carbon layers on a TiO_2 NT is found to have a lower conversion rate than that for GDN-5.

In summary, we reported a new method to fabricate a novel structure of thin island-shaped GDs with two to four sp^2-bonded carbon layers along the surface curvature of TiO_2 NTs that preserves the original ordered morphology and their anatase crystal structure. The high hydrogen generation rate on this novel catalyst shows that they can be effective as electron reservoirs for solar-driven electrons, where solar-driven electrons in the CB of TiO_2 can jump into the GDs and then be shuttled to hydrogen protons in water. Therefore, we expect that combining GDs with a broad class of semiconductors could provide an innovative means for suppressing charge recombination and promoting photocatalytic properties.

Acknowledgements

This research was supported by the Korea Center for Artificial Photosynthesis (KCAP, NRF-2012-M1A2A2671834), the WCU (World Class University) program (R-31-2008-000-10055-0), the Priority Research Centers Program (2011-0031407) and the Center for Inorganic Photovoltaic Materials (2012-0001174) funded by the Ministry of Education, Science and Technology (MEST). D. K. Lee was supported by the Hydrogen Energy R&D Center from one of the 21st Century Frontier R&D Programs, the National Research Foundation (NRF) of Korea (NRF-2011-0028737) and the Secondary Battery Program (NRF-2010-0029042) funded by the MEST.

Notes and references

1 A. Fujishima and K. Honda, *Nature*, 1972, **238**, 37–38.
2 M. R. Hoffmann, S. T. Martin, W. Y. Choi and D. W. Bahnemann, *Chem. Rev.*, 1995, **95**, 69–96.
3 C. Richter and C. A. Schmuttenmaer, *Nat. Nanotechnol.*, 2010, **5**, 769–772.
4 A. Kudo and Y. Miseki, *Chem. Soc. Rev.*, 2009, **38**, 253–278.
5 S. C. Roy, O. K. Varghese, M. Paulose and C. A. Grimes, *ACS Nano*, 2010, **4**, 1259–1278.
6 F. Jiao and H. Frei, *Angew. Chem., Int. Ed.*, 2009, **48**, 1841–1844.
7 M. Kitano, K. Tsujimaru and M. Anpo, *Top. Catal.*, 2008, **49**, 4–17.
8 M. Batzill, *Energy Envion. Sci.*, 2011, **4**, 3275–3286.
9 P. V. Kamat, I. Bedja and S. Hotchandani, *J. Phys. Chem.*, 1994, **98**, 9137–9142.
10 K. Woan, G. Pyrgiotakis and W. Sigmund, *Adv. Mater.*, 2009, **21**, 2233–2239.
11 R. Leary and A. Westwood, *Carbon*, 2011, **49**, 741–772.
12 P. V. Kamat, *J. Phys. Chem. Lett.*, 2011, **2**, 242–251.
13 Y. Sun, Q. Wu and G. Shi, *Energy Environ. Sci.*, 2011, **4**, 1113–1132.
14 A. K. Geim and K. S. Novoselov, *Nature*, 2007, **6**, 183–191.
15 H. Zhang, X. Lv, Y. Li, Y. Wang and J. Li, *ACS Nano*, 2009, **4**, 380–386.
16 X. Sun and Y. Li, *Angew. Chem., Int. Ed.*, 2004, **43**, 597–601.
17 J. Lee, J. Kim and T. Hyeon, *Adv. Mater.*, 2006, **18**, 2073–2094.
18 P. Roy, S. Berger and P. Schmuki, *Angew. Chem., Int. Ed.*, 2011, **50**, 2904–2939.

19 D. Gong, C. A. Grimes, O. K. Vargese, W. Hu, R. S. Singh, Z. Chen and E. C. Dickey, *J. Mater. Res.*, 2001, **16**, 3331–3334.
20 K. S. Han, D. K. Lee, J. W. Lee, G. I. Lee and J. K. Kang, *Chem.–Eur. J.*, 2011, **17**, 2579–2582.
21 M. Myahkostupov, M. Zamkov and F. N. Castellano, *Energy Envrion. Sci.*, 2011, **4**, 998–1010.
22 J. Robertson, *Mater. Sci. Eng., R*, 2002, **37**, 129–281.
23 A. Corras, G. Mountjoy, D. Gozzi and A. Latini, *Nanotechnology*, 2007, **18**, 485610.
24 H. Qian, S. Yu, L. Luo, J. Gong, L. Fei and X. Liu, *Chem. Mater.*, 2006, **18**, 2102–2108.
25 J. C. Heckel, F. F. Farhan and G. Chumanov, *Colloid Polym. Sci.*, 2008, **286**, 1545–1552.
26 A. C. Ferrari, J. C. Meyer, V. Scardaci, C. Casiraghi, M. Lazzeri, F. Mauri, S. Piscanec, K. S. Novoselov, S. Roth and A. K. Geim, *Phys. Rev. Lett.*, 2006, **97**, 187401.
27 A. C. Ferrari and J. Robertson, *Phys. Rev. B: Condens. Matter Mater. Phys.*, 2000, **61**, 14095.
28 L. A. Pesin, *J. Mater. Sci.*, 2002, **37**, 1–28.
29 M. Phaner-Goutorbe, A. Sartre and L. Porte, *Microsc., Microanal., Microstruct.*, 1994, **5**, 283–290.
30 O. Akhavan, M. Abdolahad, A. Esfandiar and M. Mohatashamifar, *J. Phys. Chem. C*, 2010, **114**, 12955–12959.
31 P. Merel, M. Tabbai, M. Chaker, S. Moisa and J. Margot, *Appl. Surf. Sci.*, 1998, **136**, 105–110.
32 A. Kongkanand, K. Tvrdy, K. Takechi, M. Kuno and P. V. Kamat, *J. Am. Chem. Soc.*, 2008, **130**, 4007–4015.
33 N. Yang, J. Zhai, D. Wang, Y. Chen and L. Jiang, *ACS Nano*, 2010, **4**, 887–894.
34 S. Krishanamurthy, I. V. Lightcap and P. V. Kamat, *J. Photochem. Photobiol., A*, 2011, **221**, 214–219.
35 B. Chang and S. Park, *Annu. Rev. Anal. Chem.*, 2010, **3**, 207–229.
36 P. Pu, H. Cachet and E. M. M. Sutter, *Electrochim. Acta*, 2010, **55**, 5938–5946.
37 F. Fabregat-Santiago, J. Bisquert, E. Palomares, L. Otero, D. Kuang, S. M. Zakeeruddin and M. Gratzel, *J. Phys. Chem. C*, 2007, **111**, 6550–6560.
38 F. Fabregat-Santiago, E. M. Barea, J. Bisquert, G. K. Mor, K. Shankar and C. A. Grimes, *J. Am. Chem. Soc.*, 2008, **130**, 11312–11316.
39 X. He, Y. Cai, H. Zhang and C. Liang, *J. Mater. Chem.*, 2011, **21**, 475–480.
40 W. Fan, Q. Lai, Q. Zhang and Y. Wang, *J. Phys. Chem. C*, 2011, **115**, 10694–10701.
41 M. Shen and M. A. Henderson, *J. Phys. Chem. Lett.*, 2011, **2**, 2707–2710.
42 T. Puangpetch, T. Sreethawong, S. Yoshikawa and S. Shavadej, *J. Mol. Catal. A: Chem.*, 2009, **312**, 97–106.